MAGNETIC FIELDS FROM QCD PHASE TRANSITIONS

Alexander G. Tevzadze[1], Leonard Kisslinger[2], Axel Brandenburg[3,4], and Tina Kahniashvili[2,5,6]

[1] Faculty of Exact and Natural Sciences, Javakhishvili Tbilisi State University, 1 Chavchavadze Avenue, Tbilisi 0128, Georgia; aleko@tevza.org
[2] McWilliams Center for Cosmology and Department of Physics, Carnegie Mellon University, 5000 Forbes Avenue, Pittsburgh, PA 15213, USA
[3] Nordita, KTH Royal Institute of Technology and Stockholm University, Roslagstullsbacken 23, SE-10691 Stockholm, Sweden
[4] Department of Astronomy, AlbaNova University Center, Stockholm University, SE-10691 Stockholm, Sweden
[5] Department of Physics, Laurentian, University, Ramsey Lake Road, Sudbury, ON P3E 2C, Canada
[6] Abastumani Astrophysical Observatory, Ilia State University, 3-5 Cholokashvili Street, Tbilisi 0194, Georgia

ABSTRACT

We study the evolution of QCD phase transition-generated magnetic fields (MFs) in freely decaying MHD turbulence of the expanding universe. We consider an MF generation model that starts from basic non-perturbative QCD theory and predicts stochastic MFs with an amplitude of the order of 0.02 μG and small magnetic helicity. We employ direct numerical simulations to model the MHD turbulence decay and identify two different regimes: a "weakly helical" turbulence regime, when magnetic helicity increases during decay, and "fully helical" turbulence, when maximal magnetic helicity is reached and an inverse cascade develops. The results of our analysis show that in the most optimistic scenario the magnetic correlation length in the comoving frame can reach 10 kpc with the amplitude of the effective MF being 0.007 nG. We demonstrate that the considered model of magnetogenesis can provide the seed MF for galaxies and clusters.

Key words: early universe – magnetic fields

Online-only material: color figures

1. INTRODUCTION

The origin of the observed magnetic fields (MFs) in galaxies and clusters of $\sim 10^{-6}$–10^{-5} G remains a matter of debate (Beck et al. 1996; Widrow 2002; Vallée 2004). Recently several different groups (Neronov & Vovk 2010; Tavecchio et al. 2010; Dolag et al. 2011; Taylor et al 2011; Huan et al. 2011) reported the detection of a lower bound on a large-scale correlated MF amplitude of the order of 10^{-16}–10^{-15} G, or possibly two orders of magnitude smaller (Dermer et al. 2011; Takahashi et al. 2012) at Mpc scales through blazar observations. One of the possible explanations of the large-scale correlated MF assumes the presence of a seed primordial magnetic field (PMF) which was generated during or prior to the radiation-dominated epoch. This MF should satisfy several conditions: (1) the PMF should preserve approximate spatial isotropy, it has to be weak enough when its energy density can be treated as a first order of perturbation; (2) the PMF should be smaller than the MF in galaxies by a few orders of magnitude at least, since during structure formation PMFs get amplified; (3) since the PMF energy density ρ_B contributes to the radiation field, the big bang nucleosynthesis bound implies $\Omega_B h_0^2 = \rho_B/\rho_{cr} \leqslant 2.4 \times 10^{-6}$ (Grasso & Rubinstein 2001), where ρ_{cr} is the critical density,[7] and h_0 is the Hubble constant in units of 100 km s^{-1} Mpc^{-1}.

The possible origin of the PMF from the two major cosmological phase transitions, the electroweak phase transition (EWPT) and the QCD phase transition (QCDPT; see Grasso & Rubinstein 2001; Widrow 2002; Widrow et al. 2012 for reviews) is of particular importance for cosmology. Because of the larger scale of the resulting seed MF and the nature of the QCD bubble walls during a first-order QCDPT, it is more likely that the

QCDPT rather than the EWPT produces a PMF that accounts for the observed galactic and cluster MFs.

In this paper, we consider one of several possible mechanisms of PMF generation. In particular we re-address the model proposed by Kisslinger (2003), in which the PMF is generated via QCD bubble collisions. We consider the coupling of this initial PMF with the QCD plasma, and study the dynamics during the expansion of the universe. The main parameters of the described model are given by the QCDPT temperature $T_\star = 0.15$ GeV and the number of relativistic degrees of freedom $g_\star = 15$. The interactions between the PMF and the QCD plasma are studied through numerical MHD simulations using the Pencil Code (see http://pencil-code.googlecode.com/). We discuss observational signatures of such a QCDPT PMF, including observed MFs in galaxies and clusters. We employ natural units with $\hbar = 1 = c$ and Gaussian units for the MHD formulation.

The outline of the paper is as follows. In Section 2, we describe the PMF generation model. In Section 3, we determine the spatial and temporal characteristics of the generated PMF. The results of our analysis, including the dynamics of the PMF, are presented in Section 4, where we discuss the resulting MF in galaxies and clusters. Conclusions are presented in Section 5.

2. MAGNETIC FIELD GENERATION MODEL

In contrast to the EWPT, the QCDPT involves the treatment of QCD, which, unlike the electroweak theory, is non-perturbative. Therefore a valid theory starting from basic QCD theory, rather than a model, must be able to treat non-perturbative QCD. In Kisslinger (2003), instantons form gluonic bubble walls and it is the interior gluonic wall that leads to the magnetic seed described below satisfying that criterion. In this early work, the main interest was the prediction of polarization correlations in cosmic microwave background radiation (CMBR). As we can see below the magnitude of the resulting MF is too small for current CMBR observations, but it might be measured in the

---

[7] The ratio of ρ_B to the energy density of the radiation ρ_{rad} is constant during cosmological evolution if the PMF is not damped by an MHD (or other) process and therefore stays frozen into the plasma.

future. Because this scenario starts from basic non-perturbative QCD theory and successfully predicts a primary MF which has the overall properties that are promising for the PMF, we use it in our present work.

In this section, we briefly describe the PMF scenario proposed by Kisslinger (2003). In Section 2.1 we review the MF and helicity density created during the QCDPT, and in Section 2.2 we give values of these quantities at the present time. Recent lattice QCD studies have shown that the QCDPT is first order, so bubbles form and collide (see De Risi et al. 2008; Fraga & Misher 2009; Bessa et al. 2009; Schwarz & Stuke 2009; Schettler et al. 2011; Boeckel & Schaffner-Bielich 2011, and references therein); additional references are given by Kahniashvili et al. (2010b). The first-order QCDPT can result in the generation of an MF through two (or more) bubble collisions.

2.1. Magnetic Field and Helicity During the QCDPT

The QCD phase transition critical temperature is defined as $T_\star \simeq 0.15$ GeV. A gluonic wall is created as two bubbles collide, and a magnetic wall is formed by the interaction of the nucleons with the gluonic wall. The electromagnetic interaction Lagrangian is

$$\mathcal{L}^{\text{int}} = -e\bar{\Psi}\gamma^\mu A_\mu^{\text{em}}\Psi, \tag{1}$$

where Ψ is the nucleon field operator, A^{em} is the electromagnetic 4-potential, and γ^μ are the Dirac matrices. In Kisslinger (2003), it was shown that the interaction of the quarks in the nucleons with the gluonic wall aligns the nucleon magnetic dipole moments, producing a B-field orthogonal to the gluonic wall.

Using an instanton model for the gluonic wall oriented in the x–y direction (say), one obtains for $B_z(\boldsymbol{x})$ at the time of the QCDPT, with $T = T_\star$,

$$B_z(\boldsymbol{x}) = B_\star^{(\text{QCD})} e^{-b^2(x^2+y^2)} e^{-M_n^2 z^2}, \tag{2}$$

where $b^{-1} = d_H \simeq$ a few km = horizon size at the end of the QCDPT ($t \simeq 10^{-4}$ s) and $M_n^{-1} = 0.2$ fm. $B_\star^{\text{QCD}}$, the magnitude of the MF within the wall of thickness ζ, is (see Kisslinger 2003)

$$B_\star^{(\text{QCD})} \simeq \frac{1}{\zeta\,\Lambda_{\text{QCD}}} \frac{e}{2M_n} \times \langle\bar{\Psi}\sigma_{21}\gamma_5\Psi\rangle, \tag{3}$$

where $\Lambda_{\text{QCD}} \simeq 0.15$ GeV is the QCD momentum scale, $\gamma_5 = i\gamma^0\gamma^1\gamma^2\gamma^3$, and $\sigma_{21} = i\gamma_2\gamma_1 = i\gamma^2\gamma^1$. A similar form had been derived earlier using the domain wall model of Forbes & Zhitnitsky (2000). The value for $B^{(\text{QCD})}$ was found to be

$$B_\star^{(\text{QCD})} \simeq 0.39\frac{e}{\pi}\Lambda_{\text{QCD}}^2 \simeq 1.5 \times 10^{-3}\,\text{GeV}^2 \simeq 2.2 \times 10^{16}\,\text{G}. \tag{4}$$

The asterisk indicates that we refer to the *initial* value of the MF at the time of the QCDPT.

We now discuss the magnetic helicity created during the QCDPT using the scenario proposed by Kisslinger (2003). Magnetic helicity is an important characteristic that strongly influences the PMF dynamics. Magnetic helicity is a conserved quantity during the subsequent evolution past the QCDPT. This leads to an inverse cascade producing MFs at progressively larger scales. For this to work, it is important to know the magnetic helicity that is produced by the QCDPT.

The magnetic helicity is defined as $\int d^3x\,\boldsymbol{A}\cdot\boldsymbol{B}$, with $\boldsymbol{B} = \nabla\times\boldsymbol{A}$. In the domain wall model of Forbes & Zhitnitsky (2000), the magnetic helicity density $\mathcal{H}_M$ is

$$\mathcal{H}_M = \boldsymbol{A}\cdot\boldsymbol{B} = A_z B_z, \tag{5}$$

for a PMF in the z-direction, as discussed above. Because of the violation of charge conjugation and parity invariance of the strong force (strong CP violation) during the QCDPT, magnetic helicity is produced through the alignment of magnetic and electric dipole moments of the nucleons. Thus, the electric field satisfies $E_z \simeq B_z$ (see Forbes & Zhitnitsky 2000). From Maxwell's equations in the Weyl gauge we have

$$\boldsymbol{E} = -\frac{1}{c}\frac{\partial\boldsymbol{A}}{\partial t} \quad\text{or}\quad A_z \simeq -E_z\tau, \tag{6}$$

where $\tau \simeq 1/\Lambda_{\text{QCD}}$ is the timescale for the QCDPT. From Equations (5) and (6) one finds

$$\begin{aligned}\mathcal{H}_{M,\star}^{\text{QCD}} &\simeq B_z^2/\Lambda_{\text{QCD}} \\ &\simeq (0.22\times10^{17}\,\text{G})^2/(0.15\,\text{GeV}), \end{aligned} \tag{7}$$

where we have assumed statistical homogeneity, so the result is gauge-independent.

2.2. Comoving Values of Magnetic Field and Helicity

The simple dilation due to the expansion of the universe significantly reduces the amplitude of both the MF and the magnetic helicity created during the QCDPT. Defining $a_\star$ and a_0 as the scale factors at the time of the QCDPT and today, respectively, we have

$$\frac{a_\star}{a_0} \simeq 10^{-12}\left(\frac{0.15\,\text{GeV}}{T_\star}\right)\left(\frac{15}{g_\star}\right)^{1/3}, \tag{8}$$

with $g_* = 15$, $T_\star = 0.15$ GeV.

The comoving (present) value of the PMF field B_{in} (the subscript "in" indicates that the QCD field is an initial PMF for further developed MHD dynamics) is given by $B_{\text{in}} = (a_\star/a_0)^2 \times B_\star^{(\text{QCD})}$, which results in

$$B_{\text{in}} \simeq 2 \times 10^{-8}\,\text{G}. \tag{9}$$

As in the case of the PMF amplitude, magnetic helicity density experiences dilution due to the expansion of the universe. The comoving (initial) value of the magnetic helicity density is given by

$$\mathcal{H}_{M,\text{in}} = \left(\frac{a_\star}{a_0}\right)^3 \times \mathcal{H}_{M,\star}^{\text{QCD}} \simeq 10^{-39}(\text{G}^2\cdot\text{Mpc}). \tag{10}$$

This value is extremely small, and it is almost $\times10^{19}$ smaller than the maximal allowed magnetic helicity (see below). Such a small value of magnetic helicity density is due to the thickness of the magnetic wall; see Equation (2) and Kisslinger (2003). On the other hand, several studies indicate strong CP violation during QCDPT (Kharzeev 2006; Voloshin 2004; Creutz 2011). In this case magnetic helicity can reach its maximal value, if we assume the MF to be correlated over the Hubble scale $\lambda_{H_\star}$, as will be explained below. Being more conservative we assume that the MF correlation should coincide with the bubble size ξ_M, see Section 3. The resulting magnetic helicity will then be smaller than the maximal one by a factor of the order of $\xi_M/\lambda_{H_\star}$. As we will see in Section 4, the duration of the process is long enough to ensure that the maximal value of magnetic helicity is reached during the subsequent evolution.

3. MAGNETIC FIELD SPECTRUM

Following our earlier studies (Kahniashvili et al. 2010a), we treat the initial PMF energy density $\mathcal{E}_M$ as magnetic energy density injected into the cosmological plasma at the comoving length scale λ_0 which corresponds to the QCD bubble size. We recall that the PMF has been generated on the thin surfaces between colliding bubbles, while the correlation length scale of this PMF might be associated with the bubble length scale. In the following, we assume that the PMF spectrum in Fourier space is sharply peaked at $k_0 = 2\pi/\lambda_0$. After generation, the PMF evolution (during the PT) depends sensitively on the length scale under consideration and on the presence of magnetic helicity (see Harrison 1970; Turner & Widrow 1988; Cornwall 1997; Jackiw & Pi 2000; Garretson et al. 1992; Field & Carroll 2000; Giovannini 2000; Vachaspati 2001; Campanelli 2007, 2009; Durrer et al. 2011 for magnetic helicity generation mechanisms). The expansion of the universe leads to additional effects, in particular to a faster growth of the PMF correlation length. A distinctive effect is the different time behavior of the PMF decay.

In the cosmological context most important is the difference between the growth of the comoving length scale ($L \propto a$) and the Hubble radius ($H^{-1} \propto t$, where t is physical time). This leads to additional effects in the PMF evolution (and damping) (see Son 1999; Banerjee & Jedamzik 2003; Caprini et al. 2009). Note that to describe properly the dynamics of the perturbations in the expanding universe, it is appropriate to switch to comoving quantities and to describe the processes in terms of conformal time η (Brandenburg et al. 1996). After this procedure, the MHD equations include the effects of the expansion while retaining their conventional flat spacetime form. To keep the description as simple as possible we work with dimensionless quantities, such as the normalized wavenumber[8] $\gamma = \lambda_0/H_\star^{-1}$ and normalized energy density defined below.

The coupling between the PMF and the plasma leads to a spreading of the fixed scale PMF over a wide range of length scales, thus forming the PMF spectrum. After a few turnover times the modified PMF spectrum is established (see Section 4 for details of the simulations).

To show the coupling between the initial PT-generated MF and the plasma we give here the basic MHD equations for an incompressible conducting fluid (Biskamp 2003):

$$\left[\frac{\partial}{\partial \eta} + (\boldsymbol{v} \cdot \boldsymbol{\nabla}) - \nu \nabla^2 \right] \boldsymbol{v} = (\boldsymbol{b} \cdot \boldsymbol{\nabla})\boldsymbol{b} - \boldsymbol{\nabla} p + \boldsymbol{f}_K, \quad (11)$$

$$\left[\frac{\partial}{\partial \eta} + (\boldsymbol{v} \cdot \boldsymbol{\nabla}) - \lambda \nabla^2 \right] \boldsymbol{b} = (\boldsymbol{b} \cdot \boldsymbol{\nabla})\boldsymbol{v} + \boldsymbol{\nabla} \times \boldsymbol{f}_M, \quad (12)$$

with $\boldsymbol{\nabla} \cdot \boldsymbol{b} = 0$, where η is the conformal time, $\boldsymbol{v}(\boldsymbol{x}, \eta)$ is the fluid velocity, $\boldsymbol{b}(\boldsymbol{x}, \eta) \equiv \boldsymbol{B}(\boldsymbol{x}, \eta)/\sqrt{4\pi w}$ is the normalized MF, $\boldsymbol{f}_K(\boldsymbol{x}, \eta)$ and $\boldsymbol{f}_M(\boldsymbol{x}, \eta)$ are external forces driving the flow and the MF ($\boldsymbol{f}_K = \boldsymbol{f}_M = 0$ for the results presented below, but $\boldsymbol{f}_M \neq 0$ for producing initial conditions), ν is the comoving viscosity of the fluid, λ is the comoving resistivity, $w = \rho + p$ is the enthalpy, ρ is the energy density, and p is the pressure of the plasma. Here we are interested in the radiation-dominated epoch.

To proceed we derive the Fourier transform of the PMF two-point correlation function as

$$\langle b_i^*(\boldsymbol{k}, \eta) b_j(\boldsymbol{k}', \eta + \tau) \rangle = (2\pi)^3 \delta(\boldsymbol{k} - \boldsymbol{k}') F_{ij}^M(\boldsymbol{k}, \tau).f[\kappa(k), \tau], \tag{13}$$

Such a presentation allows a direct analogy with hydrodynamic turbulence (Landau & Lifshitz 1987). In fact, b_i represents the Alfvén velocity. The normalized energy density of the PMF is then $\mathcal{E}_M = \langle \boldsymbol{b}^2 \rangle/2$, while the kinetic energy density is $\mathcal{E}_K = \langle \boldsymbol{v}^2 \rangle/2$, and the spectral correlation tensor is

$$\frac{F_{ij}^M(\boldsymbol{k}, \tau)}{(2\pi)^3} = P_{ij}(\boldsymbol{k}) \frac{E_M(k, \tau)}{4\pi k^2} + i\varepsilon_{ijl} k_l \frac{H_M(k, \tau)}{8\pi k^2}. \tag{14}$$

Here, $P_{ij}(\boldsymbol{k}) = \delta_{ij} - k_i k_j/k^2$ is the projection operator, δ_{ij} is the Kronecker delta, $k = |\boldsymbol{k}|$, ε_{ijl} is the totally antisymmetric tensor, and $\kappa(k)$ is an autocorrelation function that determines the characteristic function $f[\kappa(k), \tau]$ describing the temporal decorrelation of turbulent fluctuations. The function $H_M(k, \eta)$ is the magnetic helicity spectrum. Note that $E_M(k) = k^2 P_B(k)/\pi^2$, where $P_B(k)$ is the MF power spectrum.

The power spectra of magnetic energy $E_M(k, \eta)$ and magnetic helicity $H_M(k, \eta)$ are related to magnetic energy density and helicity density through $\mathcal{E}_M(\eta) = \int_0^\infty dk E_M(k, \eta)$ and $\mathcal{H}_M(\eta) = \int_0^\infty dk H_M(k, \eta)$, respectively. The magnetic correlation length,

$$\xi_M(\eta) = \frac{1}{\mathcal{E}_M(\eta)} \int_0^\infty dk \, k^{-1} E_M(k, \eta), \tag{15}$$

corresponds to the largest eddy length scale. All configurations of the MF must satisfy the "realizability condition" (Biskamp 2003)

$$|\mathcal{H}_M(\eta)| \leqslant 2\xi_M(\eta)\mathcal{E}_M(\eta). \tag{16}$$

Also, the velocity energy density spectrum $E_K(k, \eta)$ is related to the kinetic energy of the turbulent motions through $\mathcal{E}_K(\eta) = \int_0^\infty dk \, E_K(k, \eta)$.

One of the main characteristics of the PMF is the correlation length and its growth. The maximal correlation length $\xi_{\max}$ for a causally generated PMF cannot exceed the Hubble radius[9] at the time of generation $H_\star^{-1}$. The comoving length corresponding to the Hubble radius at generation is inversely proportional to the temperature $T_\star$,

$$\lambda_{H_\star} = 5.3 \times 10^{-7} \, \text{Mpc} \left(\frac{0.15 \, \text{GeV}}{T_\star} \right) \left(\frac{15}{g_\star} \right)^{1/6}, \tag{17}$$

and is equal to 0.5 pc for the QCDPT with $g_\star = 15$ and $T_\star = 0.15$ GeV.

The PMF spectrum is characterized not only by its spatial distribution, but also by its characteristic times: (1) the largest-size eddy turnover time $\tau_0 \simeq l_0/v_A$ (where v_A is the rms Alfvén velocity), which can also be used to determine the minimal duration of the source needed to justify the use of the stationary turbulence approximation (Proudman 1952; Monin & Yaglom 1975); (2) the direct cascade timescale of the turbulence τ_{dc}; and (3) the large-scale turbulence decay time τ_{ls}.

The temporal characteristics of the MHD turbulence are given through the form of $f(\kappa(k), \tau)$, which is due to the

---

[8] Here the subscript $\star$ indicates again the moment of the PMF generation. γ can be associated with the number of PMF bubbles within the Hubble radius, $N \propto \gamma^3$. This value depends on the PT model: for the QCDPT we assume $\gamma \simeq 0.15$.

[9] The inflation-generated PMF (Turner & Widrow 1988; Ratra 1992) correlation length can exceed the Hubble horizon today.

complex process of MHD turbulence decorrelation (Terry & Smith 2007) and is currently not fully understood. To proceed we employ Kraichnan's approach (Kraichnan 1964) and specify the decorrelation function $f_{dc}[\kappa(k_{ph}), \tau] = \exp[-\pi\kappa^2(k_{ph})\tau^2/4]$ defined within the inertial range, $k_0 < k < k_d$. Here τ is the duration of the turbulence process and $\kappa(k_{ph}) = \bar{\varepsilon}_M^{1/3} k_{ph}^{2/3}/\sqrt{2\pi}$, where k_{ph} is the physical wavenumber related to the comoving k through $k_{ph}(a) = k a_0/a$ (a_0 is the value of the scale factor now), and $\bar{\varepsilon}_M$ is the proper dissipation rate per unit enthalpy. Hence, we have (Kahniashvili et al. 2011)

$$f_{dc}[\bar{k}, \tau] = \exp\left[-\frac{2\pi^2}{9}\left(\frac{\tau}{\tau_0}\right)^2 \bar{k}^{4/3}\right]. \qquad (18)$$

Here, $\bar{k} = k/k_0$ is the normalized wavenumber and τ_0 corresponds to the largest eddy turnover time. It is clear that after switching off the forcing, the turbulent motions are decorrelated within a few turnover times, and are in fact irrelevant to influence the large-scale MF.

4. GROWTH OF CORRELATION LENGTH IN HELICAL TURBULENCE

To assess the importance of a small initial magnetic helicity, we perform direct numerical simulations of decaying MHD turbulence with an initial MF of finite relative magnetic helicity using different values, and a correlation length ξ_M that is small compared with the scale of the domain λ_1.

4.1. Simulation Technique

We solve the compressible equations with the pressure given by $p = \rho c_s^2$, where $c_s = 1/\sqrt{3}$ is the sound speed for an ultrarelativistic gas. Following our earlier work (Kahniashvili et al. 2010a), we solve the equations governing equations for the logarithmic density $\ln\rho$, the velocity $\boldsymbol{v}$, and the magnetic vector potential $\boldsymbol{A}$, in the form

$$\frac{D\ln\rho}{D\eta} = -\boldsymbol{\nabla}\cdot\boldsymbol{v}, \qquad (19)$$

$$\frac{D\boldsymbol{v}}{D\eta} = \boldsymbol{J}\times\boldsymbol{B} - c_s^2\boldsymbol{\nabla}\ln\rho + \boldsymbol{f}_{visc}, \qquad (20)$$

$$\frac{\partial\boldsymbol{A}}{\partial\eta} = \boldsymbol{v}\times\boldsymbol{B} + \boldsymbol{f}_M + \lambda\nabla^2\boldsymbol{A}, \qquad (21)$$

where $D/D\eta = \partial/\partial\eta + \boldsymbol{v}\cdot\boldsymbol{\nabla}$ is the advective derivative, $\boldsymbol{f}_{visc} = \nu(\nabla^2\boldsymbol{v} + (1/3)\boldsymbol{\nabla}\boldsymbol{\nabla}\cdot\boldsymbol{v} + \boldsymbol{G})$ is the viscous force in the compressible case with constant ν and $G_i = S_{ij}\nabla_j\ln\rho$ as well as $S_{ij} = (1/2)(v_{i,j} + v_{j,i}) - (1/3)\delta_{ij}v_{k,k}$ being the trace-free rate of strain tensor. Furthermore, $\boldsymbol{J} = \boldsymbol{\nabla}\times\boldsymbol{B}/4\pi$ is the normalized current density. We emphasize that $\boldsymbol{f}_M = \boldsymbol{0}$, except for producing initial conditions, as explained below.

The bulk motions are always slow enough, so compressibility effects are not important. Similar to before, we express the MF in Alfvén units, but now based on the volume average enthalpy, i.e., $\boldsymbol{b} \equiv \boldsymbol{B}/\sqrt{4\pi\langle w\rangle}$, where $w = 4/3\rho$ for an ultrarelativistic gas. We use 512^3 mesh points in a domain of size $(2\pi)^3$, so the lowest wavenumber in the domain is $k_1 = 1$. We choose $\nu = \eta = 10^{-5}$ in units of c_s/k_1.
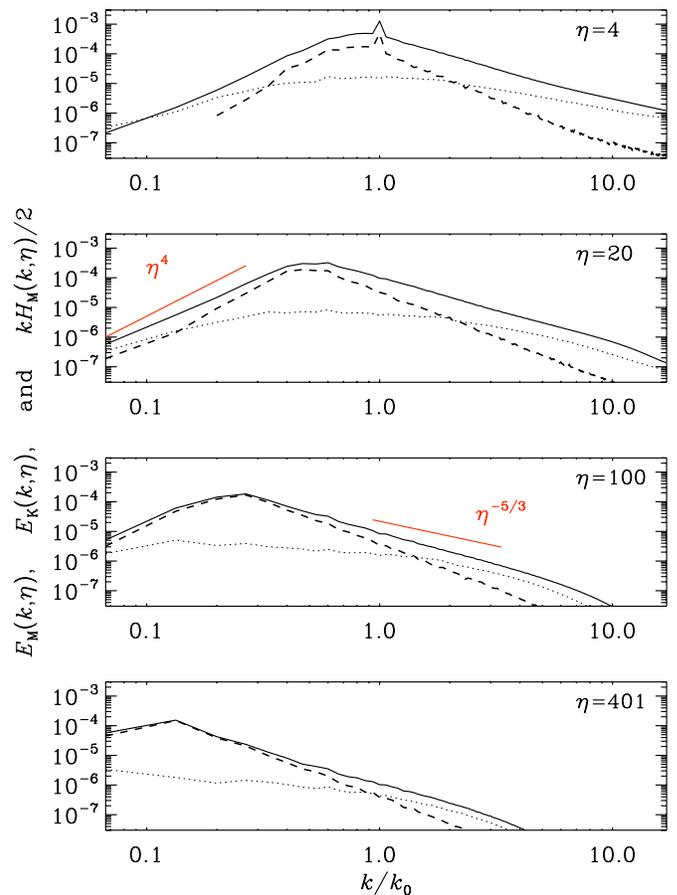

Figure 1. Spectra of magnetic energy (solid lines), kinetic energy (dotted), and magnetic helicity scaled by $k/2$ (dashed) for a run with $\sigma = 0.03$ at three different times. At early times, $H_M(k, \eta)$ can be negative at small values of k, which explains why the dashed line terminates in those cases.

(A color version of this figure is available in the online journal.)

4.2. Initial Conditions

A suitable initial condition is produced by simulating for a short time interval ($\Delta t \approx 0.5\lambda_1/c_s$) with a random δ-correlated magnetic forcing term $\boldsymbol{f}_M$ in the evolution equation for the magnetic vector potential. This forcing term consists of plane monochromatic waves with wavenumber k_0 and fractional helicity $\langle\boldsymbol{f}_M\cdot\boldsymbol{\nabla}\times\boldsymbol{f}_M\rangle/\langle k_0\boldsymbol{f}_M^2\rangle = 2\sigma/(1+\sigma^2)$; in the following we quote the value of σ. This procedure has the advantage that the magnetic and velocity fields used then for the subsequent decay calculations are obtained from a self-consistent solution to the MHD equations.

4.3. Growth of Helical Structures

In Figure 1 we show spectra of magnetic and kinetic energy, as well as the magnetic helicity scaled by $k/2$, for a run with $\sigma = 0.03$. Initially, $kH_M(k, \eta)/2$ is well below the value of $E_M(k, \eta)$. However, at later times the two approach each other at large scales. This shows that the relative magnetic helicity increases during the decay. For the four times shown in Figure 1, the rms Mach number, v_{rms}/c_s, is 0.05, 0.025, 0.012, and 0.007; b_{rms}/v_{rms} is around 3.4, and the Reynolds numbers $v_{rms}\xi_M/\nu$ are roughly 270 for all cases.

The growth of turbulent structures is particularly clear in the MF (Figure 2). The MF drives correspondingly larger scale structures also in the velocity field. However, there are also
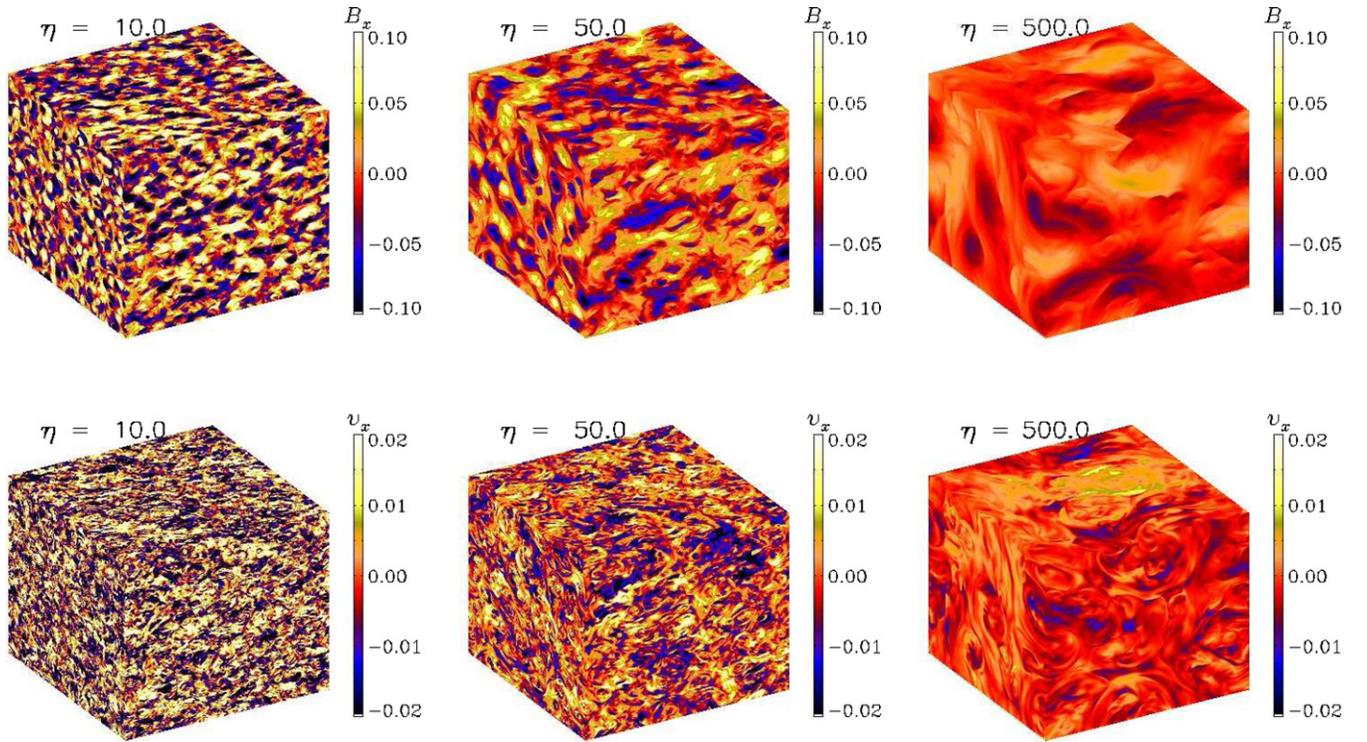
Figure 2. Visualizations of B_x (upper row) and v_x (lower row) at three times during the magnetic decay of a weakly helical field with $\sigma = 0.03$.
(A color version of this figure is available in the online journal.)

strong small-scale fluctuations in the velocity field that are not visible in the MF; see the second row of Figure 2.

In agreement with earlier simulations, we find that at small scales the magnetic energy is re-distributed by a direct cascade with a Kolmogorov-type spectrum, $E_M(k) \propto k^{-5/3}$. At large scales a Batchelor spectrum,[10] $E_M(k) \propto k^4$, is established, which was used as initial condition already in Brandenburg et al. (1996). This spectrum is in agreement with the analytical description of Durrer & Caprini (2003) who derived this result from the requirement of causality and the divergence free condition. The earlier study of Hogan (1983), which thus violates causality for magnetic energy, yielded a white noise spectrum $E(k) \propto k^2$ (Saffman spectrum) which we do observe for the spectral distribution of the kinetic energy $E_K(k) \propto k^2$.

4.4. Growth of Turbulent Length Scales

The evolution of magnetic correlation length and magnetic energy during the MHD turbulence decay can be described using two indices n_ξ and n_E:

$$\xi_M(\eta) = \xi_M(\eta_0) \left(\frac{\eta}{\eta_0} \right)^{n_\xi}, \tag{22}$$

$$\mathcal{E}_M(\eta) = \mathcal{E}_M(\eta_0) \left(\frac{\eta}{\eta_0} \right)^{n_E}. \tag{23}$$

In this case, we can model the spectral energy density of the PMF using time-dependent large- and small-scale ranges:

$$E_M(k, \eta) = E_0(\eta) \begin{cases} \bar{k}^4 & \text{when } k < k_I(\eta) \\ \bar{k}^{-5/3} & \text{when } k > k_I(\eta) \end{cases}, \tag{24}$$

---

[10] Sometimes this spectral distribution, $E_M(k) \propto k^4$, is called a von Kármán spectrum (Pope 2000).

where $\bar{k} = k/k_I$ and $k_I(\eta) = 2\pi/\xi_M(\eta)$. Hence, the evolution of the spectral amplitude E_0 for a given MF spectrum will be (see Equations (22) and (23))

$$E_0(\eta) = \frac{5}{17\pi} \xi_M(\eta_0) \mathcal{E}_M(\eta_0) \left(\frac{\eta}{\eta_0} \right)^{n_\xi + n_E}. \tag{25}$$

Magnetic helicity crucially affects the evolution of the PMF (Biskamp & Müller 1999, 2000; Son 1999; Christensson et al. 2001, 2005; Banerjee & Jedamzik 2003, 2004; Campanelli 2007). If the PMF has been generated with small magnetic helicity, there are two main stages during the development of the MF spectrum: during the first stage (sometimes called direct cascade) the PMF dynamics is similar to that of the non-helical MF. The energy cascades from large to small scales where it decorrelates and dissipates: this is a standard forward cascade development. Since magnetic helicity is conserved, its fractional value increases and thus the end of this first stage is characterized by releasing turbulence to a maximally helical state (Banerjee & Jedamzik 2003; Christensson et al. 2005) when the realizability condition (16) is reached, the inverse-cascade stage starts. The conservation of magnetic helicity implies that the magnetic energy density decays in inverse proportion to the correlation length growth during the inverse cascade. The realizability condition implies that

$$\xi_M(\eta) \geqslant \xi_M^{\min}(\eta) \equiv |\mathcal{H}_M(\eta)|/2\mathcal{E}_M(\eta), \tag{26}$$

so there is a minimum value for the correlation length. In Figure 3 we plot $\xi_M(\eta)$ and $\xi_M^{\min}(\eta)$ for $\sigma = 1, 0.1$, and 0.03. It turns out that, especially in the latter case with $\sigma = 0.03$, the increase of ξ_M remains slow ($\sim\eta^{1/2}$) as long as $\xi_M(\eta) \gg \xi_M^{\min}(\eta)$. However, since $\mathcal{H}_M$ is essentially constant and $\mathcal{E}_M$ decreases approximately like η^{-1}, the value of $\xi_M^{\min}(\eta)$ soon
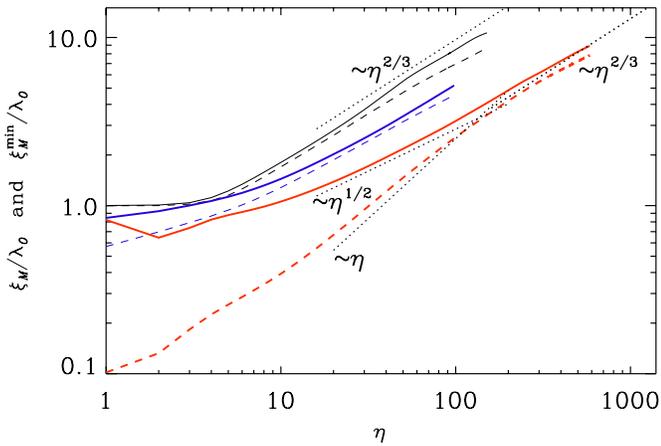
Figure 3. Evolution of $\xi_M(\eta)$ (solid) and $\xi_M^{\min}(\eta)$ (dashed) for $\sigma = 1$ (black), 0.1 (blue), and 0.03 (red).

(A color version of this figure is available in the online journal.)

Figure 4. Spectral energy density of the turbulent magnetic field $\log E_M(k)$ (color coded) in a representation of magnetic correlation length vs. temperature. The thick solid line shows the evolution of the magnetic correlation length $\xi_M(T)$. The magnetic correlation length starts to grow after the QCD phase transition at $T_\star = 0.15$ GeV, when $\xi_M = 0.075$ pc. The transparent dashed area corresponds to decorrelated magnetic field. White arrows show the direction of the evolution during the expansion of the universe. Here $n_\xi = -1/2$ and $n_E = 1$.

(A color version of this figure is available in the online journal.)

reaches $\xi_M(\eta)$. When that happens, the field is essentially fully helical and the correlation length and the magnetic energy density evolve according to $\xi_M \sim \eta^{2/3}$ and $\mathcal{E}_M \sim \eta^{-2/3}$, respectively. Hence, we recover two distinctive phases in the MHD turbulence decay process: evolution of a *weakly helical* turbulence with $n_\xi = 1/2$ and $n_E = -1$, and *fully helical* turbulence with $n_\xi = 2/3$ and $n_E = -2/3$. Note that in the latter case $E_0(\eta) \propto \xi_M(\eta)\mathcal{E}_M(\eta) = $ const (see Equation (25)) and the inverse cascade develops. Our results are in excellent agreement with Biskamp & Müller (1999), Biskamp & Müller (2000), Banerjee & Jedamzik (2003), and Campanelli (2007). The dynamical process of PMF coupling with the cosmic plasma stops at the moment of recombination after which the PMF develops more slowly (Brandenburg et al. 1997).

To calculate the time η_{fully} when a fully helical state is reached, we only need to know the initial values $\xi_M(\eta_0)$ and $\xi_M^{\min}(\eta_0)$. Since the latter approaches the former like $\eta^{1/2}$, the result is $\eta_{\text{fully}} = \eta_0[\xi_M(\eta_0)/\xi_M^{\min}(\eta_0)]^2$. Thus, in terms of the initial values of $\mathcal{E}_M$ and $\mathcal{H}_M$, a fully helical state is reached at the time

$$\eta_{\text{fully}} = 4\eta_0\xi_M^2\mathcal{E}_M^2/\mathcal{H}_M^2. \tag{27}$$

Note that this time increases quadratically with the decreasing initial value of $\mathcal{H}_M$. In case of the strong CP violation during the QCDPT, when the initial magnetic helicity can reach values that are only $\xi_M/\lambda_{H_\star}$ times less than the maximal one (see Section 2), we get $\eta_{\text{fully}} = \eta_0/\gamma^2$.

4.5. Observed Magnetic Fields

Galactic and cluster MFs are usually measured through Faraday rotation (see Vallée 2004) and, as mentioned above, the value of the coherent MF is of the order of a few μG with a typical coherence scale of 10 kpc,[11] and cluster MFs have lower limits of the order of 10^{-6} G, and at least a few nG, with similar coherence scales (Clarke et al. 2001) and additional lower limits on the steepness of the magnetic power spectrum in clusters. Furthermore, simulations starting from a constant comoving MF of 10^{-11} G suggest that MF generation in clusters can be sufficiently strong to explain Faraday rotation measurements (Dolag et al. 2002; Jedamzik & Sigl 2011).

---

[11] Strong MFs have been detected through Faraday rotation of distant quasars proving that the MFs comparable to those observed today are seen at high redshift $z \sim 3$ (Bernet et al. 2008).
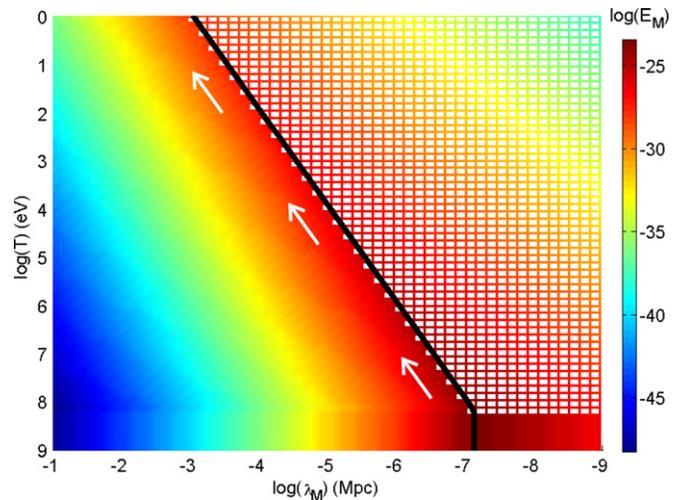
Figure 4 shows the spectral energy density of the QCDPT-generated MF (see Kisslinger 2003) with respect to temperature and correlation length in weakly helical turbulence. Initially the integral scale of the MHD turbulence is set by the QCDPT bubble scale (lower right corner of the diagram). The thick solid line marks the division between the evolution of large-scale (plain colored region) and small-scale (hashed colored region) MFs. White arrows indicate the direction of the evolution during the universe expansion. At scales below the integral scale of the turbulence, the MF undergoes exponential decorrelation, see Equation (18). The integral scale of the MHD turbulence increases, reaching $\xi_M = 1$ kpc at $T = 1$ eV. Here we have used $n_\xi = 1/2$, $n_E = -1$, with initial magnetic helicity corresponding to that given by Equation (10).

Figure 5 shows the spectral energy density of a QCDPT-generated MF in the case when the initial helical turbulence reaches the fully helical case during the expansion of the universe with $\eta_{\text{fully}}/\eta_0 = 1/(0.15)^2$. The thick solid line marks the evolution of the magnetic correlation length until the magnetic helicity reaches its maximally allowed value. In this time interval the decay law for weakly helical turbulence with $n_\xi = 1/2$ and $n_E = -1$ is applied. After the time η_{fully} when maximal magnetic helicity is reached, the correlation length follows the black dashed line and the MF evolution follows that of the fully helical case with $n_\xi = 2/3$ and $n_E = -2/3$. The integral scale of the MHD turbulence reaches $\xi_M = 10$ kpc at $T = 1$ eV.

The presented model is somewhat idealized since it ignores the time of Silk damping due to large correlation lengths for photon and neutrino viscosity (see Jedamzik & Sigl 2011). This is justified since it delays the evolution but does not destroy the field (Brandenburg et al. 1997). Therefore, we can present here only upper values for QCDPT MFs within the model by Kisslinger (2003).

The final amplitude of the MF can be estimated through two different approaches. (1) We compute the total magnetic energy
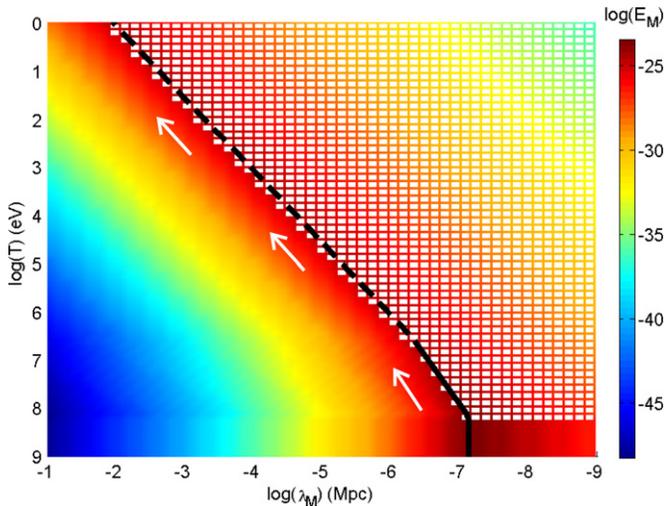
Figure 5. Similar to Figure 4, but for the case in which the magnetic field reaches a fully helical state within the considered expansion time of the universe. Initially, during the growth of magnetic helicity correlation length (solid line) and energy evolve according to $n_\xi = -1/2$ and $n_E = 1$. After reaching a fully helical state, correlation length (dashed line) and energy evolve according to $n_\xi = -2/3$ and $n_E = 2/3$.

(A color version of this figure is available in the online journal.)

density, i.e., $\mathcal{E}_M = \int_0^\infty dk \, E_M(k)$ and make the assumption that all energy is again given only at *one* scale that corresponds to the integral scale at this moment, i.e., $B_{\text{eff}} = \sqrt{8\pi\mathcal{E}_M}$. (2) Another approach is to compute the strength of the MF, $B(\lambda)$, at a given scale λ. Since observations (Vallée 2004) do not allow us to properly reconstruct the configuration of the MF we adopt first an "effective" MF approach (see Kahniashvili et al. 2011). The resulting value of the effective MF in our model of weakly helical turbulence with $\xi_M = 1$ kpc reaches 5×10^{-4} nG, while in the case of a fully helical configuration with $\xi_M = 10$ kpc we find 7×10^{-3} nG.

5. CONCLUSIONS

In this paper, we have considered QCDPT-generated PMFs and their evolution in an expanding universe accounting for the effects of MHD turbulence to explain the seed MFs of clusters and galaxies. We consider the MF generation model proposed by Kisslinger (2003), which yields an initial state of weakly helical MHD turbulence. We also study the possibility of strong CP violation according to Forbes & Zhitnitsky (2000), which yields an initial state with much higher magnetic helicity at a time when maximal helicity of the MHD turbulence is reached during the expansion of the universe. The initial seed MF is generated via QCDPT bubble collisions with a comoving correlation length of the order of 0.1 pc and with a comoving amplitude of the order of 20 nG. The initial magnetic helicity is determined by the thickness of the surface between two colliding bubbles and is extremely small if no strong CP violation is assumed (Kharzeev 2006; Voloshin 2004; Creutz 2011). During the expansion of the universe there are different processes that affect the correlation length and the strength of the MF: first of all, during the PT the field is initially peaked at a given scale and then spreads out within a wide range of wavelengths, establishing a Kolmogorov-like spectrum, $E_M(k) \propto k^{-5/3}$, at small scales and a Batchelor spectrum, $E_M(k) \propto k^4$, at large scales. If the PMF was generated without being maximally helical, the magnetic helicity experiences a steady growth. One

of the results obtained in this paper is an estimate of the timescale within which the field starts to be fully helical. In the case of an extremely weakly helical field (Kisslinger 2003), the available time to produce a fully helical PMF may be too long. The growth of the correlation length follows then a $\xi_M \propto T^{-1/2}$ law. For moderate or reasonably small initial magnetic helicity (even for $\sigma \geqslant 10^{-6}-10^{-5}$), the evolution timescale is long enough so that during the first stage of evolution, magnetic helicity grows to its maximal value. During the next stages (after magnetic helicity has reached its maximal value) the correlation length experiences a steady growth with the scaling law $\xi_M \propto T^{-2/3}$ while the energy density is decreasing in the opposite way keeping magnetic helicity almost constant. Finally, at recombination the growth of the correlation length slows down. The resulting correlation length in the most optimistic scenarios is around 10 kpc and the amplitude of the MF is around 0.007 nG. Assuming that the MF is amplified during the growth of structures (Dolag et al. 2002), such a field might well be strong enough to explain the observed MF in galaxies and clusters. On the other hand, observations of the CMB fluctuations are sensitive to PMFs of the order of a few nG (see Shaw & Lewis 2010; Yamazaki et al. 2010, and references therein).

Another possible signature of QCDPT-generated MFs is a gravitational wave signal (Kahniashvili et al. 2010b) that might be indirectly detected through pulsar timing (Durrer et al. 2011). The gravitational wave signal from PTs is usually computed assuming short duration of the source (either turbulence or PMF anisotropic stress). On the other hand, due to the free decay of MHD turbulence, the source of gravitational waves acts also after the end of PTs. For short-duration sources, the peak frequency of the gravitational waves is fully determined by the source characteristics. In particular, for QCDPT-generated gravitational waves it is far too weak to be detected though gravitational waves via ground or space-based missions. Long-duration sources might in principle substantially change the peak frequency as well as the amplitude of the signal. We plan to address this issue in future work.

REFERENCES

Banerjee, R., & Jedamzik, K. 2003, Phys. Rev. Lett., 91, 251301
Banerjee, R., & Jedamzik, K. 2004, Phys. Rev. D, 70, 123003
Beck, R., Brandenburg, A., Moss, D., Shukurov, A., & Sokoloff, D. 1996, ARA&A, 34, 155
Bernet, M. L., Miniati, F., Lilly, S. J., Kronberg, P. P., & Dessauges-Zavadsky, M. 2008, Nature, 454, 302
Clarke, T. E., Kronberg, P. P., & Böhringer, H. 2001, ApJ, 547, L111
Bessa, A., Fraga, F. S., & Mintz, B. W. 2009, Phys. Rev. D, 79, 034012

Biskamp, D. 2003, Magnetohydrodynamic Turbulence (Cambridge: Cambridge Univ. Press)
Biskamp, D., & Müller, W.-C. 1999, Phys. Rev. Lett., 83, 2195
Biskamp, D., & Müller, W.-C. 2000, Phys. Plasma, 7, 4889
Boeckel, T., & Schaffner-Bielich, J. 2011, Phys. Rev. D, 85, 103506
Brandenburg, A., Enqvist, K., & Olesen, P. 1996, Phys. Rev. D, 54, 1291
Brandenburg, A., Enqvist, K., & Olesen, P. 1997, Phys. Lett. B, 392, 395
Campanelli, L. 2007, Phys. Rev. Lett., 98, 251302
Campanelli, L. 2009, Int. J. Mod. Phys. D, 18, 1395
Caprini, C., Durrer, R., & Fenu, E. 2009, J. Cosmol. Astropart. Phys., JCAP11(2009)001
Caprini, C., Durrer, R., & Siemens, X. 2010, Phys. Rev. D, 82, 063511
Christensson, M., Hindmarsh, M., & Brandenburg, A. 2001, Phys. Rev. E, 70, 056405
Christensson, M., Hindmarsh, M., & Brandenburg, A. 2005, Astron. Nachr., 326, 393
Cornwall, J. 1997, Phys. Rev. D, 56, 6146
Creutz, M. 2011, Phys. Rev. D, 83, 016005
De Risi, G., Harko, T., Lobo, F. S. N., & Pun, C. S. J. 2008, Nucl. Phys. B, 805, 190
Dermer, C. D., Cavaldini, M., Razzaque, S., et al. 2011, ApJ, 733, L21
Dolag, K., Bartelmann, M., & Lesch, H. 2002, A&A, 387, 383
Dolag, K., Kachelriess, M., Ostapchenko, S., & Tomas, R. 2011, ApJ, 727, L4
Durrer, R., & Caprini, C. 2003, J. Cosmol. Astropart. Phys., JCAP11(2003)010
Durrer, R., Hollenstein, L., & Jain, R. K. 2011, J. Cosmol. Astropart. Phys., JCAP03(2011)037
Field, G. B., & Carroll, S. M. 2000, Phys. Rev. D, 62, 103008
Forbes, M., & Zhitnitsky, A. 2000, Phys. Rev. Lett., 85, 5268
Fraga, E. S., & Mizher, A. J. 2009, Nucl. Phys. A, 820, 103C
Garretson, W. D., Field, G. B., & Carroll, S. M. 1992, Phys. Rev. D, 46, 5346
Giovannini, M. 2000, Phys. Rev. D, 61, 063004
Grasso, D., & Rubinstein, H. R. 2001, Phys. Rev. D, 348, 163
Harrison, E. R. 1970, MNRAS, 147, 279
Hogan, C. J. 1983, Phys. Rev. Lett., 51, 1488
Huan, H., Weisgarber, T., Arlen, T., & Wakely, S. P. 2011, ApJ, 735, L28

Jackiw, R., & Pi, S. Y. 2000, Phys. Rev. D, 61, 105015
Jedamzik, K., & Sigl, G. 2011, Phys. Rev. D, 83, 103005
Kahniashvili, T., Brandenburg, A., Tevzadze, A. G., & Ratra, B. 2010a, Phys. Rev. D, 81, 123002
Kahniashvili, T., Kisslinger, L., & Stevens, T. 2010b, Phys. Rev. D, 81, 023004
Kahniashvili, T., Tevzadze, A. G., & Ratra, B. 2011, ApJ, 726, 78
Kharzeev, D. 2006, Phys. Lett. B, 633, 260
Kisslinger, L. S. 2003, Phys. Rev. D, 68, 043516
Kraichnan, R. H. 1964, Phys. Fluids, 7, 1163
Landau, L. D., & Lifshitz, E. M. 1987, Fluid Mechanics (New York: Pergamon)
Monin, A. S., & Yaglom, A. M. 1975, Statistical Fluid Mechanics (Cambridge, MA: MIT Press)
Neronov, A., & Vovk, I. 2010, Science, 328, 73
Pope, B. P. 2000, Turbulent Flows (Cambridge: Cambridge Univ. Press)
Proudman, I. 1952, Proc. R. Soc. London A, 214, 119
Ratra, B. 1992, ApJ, 391, L1
Schettler, S., Boeckel, T., & Schaffner-Bielich, J. 2011, Prog. Part. Nucl. Phys., 66, 266
Shaw, J. R., & Lewis, A. 2010, Phys. Rev. D, 81, 043517
Son, D. T. 1999, Phys. Rev. D, 59, 063008
Schwarz, D. J., & Stuke, M. 2009, J. Cosmol. Astropart. Phys., JCAP11(2009)025
Takahashi, K., Mori, M., Ichiki, K., & Inoue, S. 2012, ApJ, 744, L7
Tavecchio, F., Ghisellini, G., Foschini, L., et al. 2010, MNRAS, 406, L70
Taylor, A. M., Vovk, I., & Neronov, A. 2011, A&A, 529, A144
Terry, W. P., & Smith, K. W. 2007, ApJ, 665, 402
Turner, M. S., & Widrow, L. M. 1988, Phys. Rev. D, 37, 2743
Vachaspati, T. 2001, Phys. Rev. Lett., 87, 251302
Vallée, J. P. 2004, New Astron. Rev., 48, 763
Voloshin, S. A. 2004, Phys. Rev. C, 70, 057901
Widrow, L. M. 2002, Rev. Mod. Phys., 74, 775
Widrow, L. M., Ryu, D., Schleicher, D., et al. 2012, Space Sci. Rev., 166, 37
Yamazaki, D. G., Ichiki, K., Kajino, T., & Mathews, G. J. 2010, Adv. Astron., 2010, 586590